# Impact on Efficiency of Inductive Battery Charging System by Sub-Resonant Frequency Control during Large Variations in Coupling Conditions

*Jiayu Zhou

#Giuseppe Guidi

*,#Jon Are Suul

*Department of Engineering Cybernetics
Norwegian University of Science and Technology
Trondheim, Norway
email: jiayu.zhou@ntnu.no, jon.are.suul@ntnu.no

#SINTEF Energy Research
Trondheim, Norway
email: Giuseppe.Guidi@sintef.no

*Abstract*—**This paper presents a detailed analysis of power transfer efficiency for inductive battery charging systems designed for sub-resonant frequency control during large variations in coupling conditions. It is first demonstrated how the design for power control by sub-resonant operation allows for almost constant current amplitude and thereby constant conduction losses independently of the variations in the coupling coefficient. Since the design also can ensure slightly inductive current in the full operating range, zero voltage switching (ZVS) with very low switching losses is also ensured. Thus, the studied charging system can maintain almost constant efficiency for large variations in the magnetic coupling coefficient. A comparison with a conventionally designed inductive charging system relying on voltage control at the resonant frequency is also presented. The comparison highlights the advantages of the sub-resonant frequency control in terms of limiting component stress and maintaining a high efficiency in a wide range of coupling conditions. The efficiency characteristics that can be obtained by design for off-resonant frequency control are also demonstrated by experimental results from a small-scale laboratory prototype.**

*Keywords*—*Efficiency analysis, inductive power transfer, magnetic coupling variations, phase shift modulation, sub-resonant frequency control*

## I. INTRODUCTION

Technology for wireless inductive power transfer (IPT) has been widely studied during the last years for obtaining safe, convenient flexible and reliable battery charging in electric transportation [1]-[3]. For enabling high power application of IPT technology in electric vehicles or vessels, simple topologies with minimum number and rating of the active components are needed to limit the cost and weight of the on-board installation. Thus, the series-series (SS) compensated topology with a passive rectifier on the receiving side is usually preferred [4], [5]. However, flexible utilization of IPT technology for battery charging in large vehicles or vessels require the capability for operating in a certain range of magnetic coupling conditions. Operation of SS-compensated IPT systems at the resonance frequency implies the need for voltage control to adapt to changes in the magnetic coupling conditions [6], [7]. If the system should be capable of transferring a specified power independently of the magnetic coupling, this implies a significant need for overrating of all system components. Indeed, the maximum current required for transferring the rated power at the minimum coupling will determine the current rating while the voltage rating will be determined by the operation at the maximum coupling. Thus, the required volt-ampere rating of the converters will increase with the required range of variations in the coupling conditions that should be tolerated by the system.

To avoid this need for over-rating of components, a design approach for SS-compensated IPT systems based on sub-resonant frequency control was proposed in [8]. This design approach allowed for minimizing the component ratings while allowing for maintaining constant power transfer over a wide range of coupling conditions. It was also shown in [8] and [9] that global close-to-ideal zero voltage switching (ZVS) conditions at rated power can be ensured by slightly detuning the resonant frequencies of the sending and pickup coils. However, the sub-resonant frequency control implies operation away from the conditions that would correspond to the maximum theoretical efficiency of an ITP system. While it was generally argued in [8] and [9] that the efficiency at rated power would not be significantly influenced by the off-resonant operation, no detailed quantitative analysis of efficiency was presented.

In this paper, the impact of sub-resonant frequency control as proposed in [8] [9] on the efficiency of an IPT system with constant voltage load (CVL) is systematically evaluated for operation in a wide range of coupling conditions. It will be shown how the operation with almost constant current at constant input/output voltage allows for maintaining constant power losses independently of the frequency control. In contrast, the efficiency of a system designed for voltage control at the resonant frequency will be significantly reduced for operation at low coupling conditions with high currents and low voltages. Finally, the validity of the presented efficiency
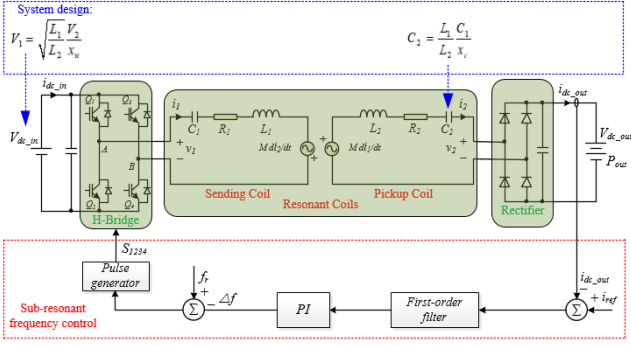
Fig. 1. System design and sub-resonant frequency control strategy of SS-compensated IPT system with constant voltage load.
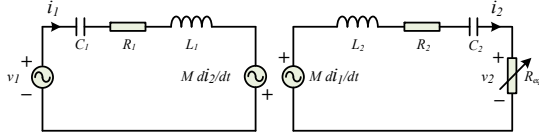


Fig. 2. Equivalent circuit of SS-compensated IPT system using harmonic approximation and equivalent load resistance.

analysis of IPT systems designed for sub-resonant frequency control are verified by simulations and experimental results obtained from a laboratory prototype.

## II. DESIGN OF SS COMPENSATED IPT SYSTEM FOR SUB-RESONANT OPERATION WITH CVL

The topology of a typical SS compensated IPT system is shown in Fig. 1, where $v_1$ ($v_2$), $i_1$ ($i_2$), $L_1$ ($L_2$), $C_1$ ($C_2$), and $R_1$ ($R_2$) are the sending coil (pickup coil) voltage, current, inductance, capacitance, and equivalent resistance, respectively, and M is the mutual inductance. A diode rectifier is assumed at the pickup side to reduce system cost and complexity, with dc terminals connected to a battery modelled as a constant voltage load $V_{dc\_out}$.

Based on a first harmonic approximation, the equivalent circuit of a typical SS compensated IPT system is shown in Fig. 2. It is worth noting that amplitude of the load voltage $V_2$ will remain constant ($V_2 = 2\sqrt{2}V_{dc\_out}/\pi$) but with a phase angle determined by the load current $I_2$, while the phase and amplitude of $I_2$ will change when the excitation frequency changes. Such CVL conditions can also cause signficant differences in the dynamic response and small-signal dynamic of the system compared to operation with a resistive load. Therefore, the output load cannot be simply modeled by an equivalent constant resistance when studying the frequency characteristics of the IPT system with CVL [10]. In this case, the relationship between the output power and frequency should be explicitly evaluated:

$$\begin{cases} V_1 = (j\omega L_1 + \dfrac{1}{j\omega C_1} + R_1)I_1 - j\omega M I_2 \\ V_2 = -(j\omega L_2 + \dfrac{1}{j\omega C_2} + R_2)I_2 + j\omega M I_1 \end{cases} \quad (1)$$

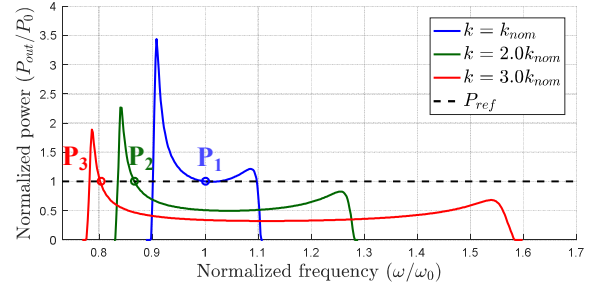$$\Rightarrow \quad P_{out} = V_2 I_2 = \frac{V_2^2}{R_{eq}(\omega, x_u, R_1, R_2)}$$



Fig. 3. IPT characteristics and operating points ($P_1$, $P_2$ and $P_3$) at rated power, constant I/O voltage, variable coupling; coils with $k_{nom}= 0.2$, unbalance factor $x_u = 0.98$, detuning factor $x_c= 1.03$.

where $x_u = \sqrt{\dfrac{L_1}{L_2}}\dfrac{V_2}{V_1}$

The equivalent load resistance $R_{eq}(\omega, x_u, R_1, R_2)$ is a complicated equation, which is not shown here due to space constraints. However, as demonstrated in [9], a simple expression of the output power can be obtained under the assumption of lossless coils ($R_1=R_2=0$):

$$P_{out} = \frac{V_2^2 \sqrt{\omega^2(\dfrac{k^2}{x_u^2}-1)+2\omega_0^2 - \dfrac{\omega_0^4}{\omega^2}}}{L_2(\omega^2(k^2-1)+2\omega_0^2 - \dfrac{\omega_0^4}{\omega^2})} \quad (2)$$

This expression ideally tends to infinite at sub- and super-resonant frequencies. However, when system losses are considered, the power transfer characteristics has two off-resonant peaks that can be utilized for power control at higher than nominal coupling. According to equation (2), a small amount of unbalance (when $x_u<1$) is very effective in increasing the power regulation range in the sub-resonant region. Such unbalance also enhances the bifurcation in the phase characteristics of the system. Moreover, global ZVS conditions at rated power can be ensured by designing the system with the resonant freqency of the pcikup coil slightly higher than that of the sending coil (i.e. design with a detuning factor $x_c=(C_1*L_1)/(C_2*L_2)>1$) [9].

Based on the design approach summarized above, the resulting IPT characteristics and operating points at rated power for different values of coupling coefficient $k$ are plotted in Fig. 3. As can be seen in the figure, the rated power can be regulated beyond the bifurcation limit of the system by controlling the operating frequency in the sub-resonant frequency region. Moreover, the phase angle of the input
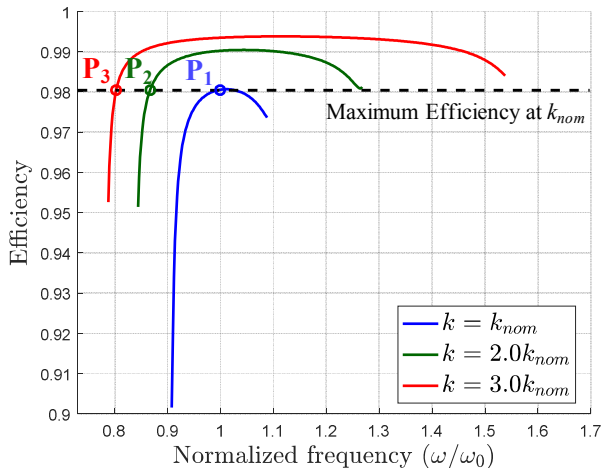
Fig. 4. The transfer efficiency of resonant network. Coils with $k_{nom}$=0.2, $Q_1$=510 and $Q_2$=490.

equivalent impedance of the system at rated power is positive with a low and almost constant value. Thus the IPT system can minimize the rating requirements of the H-bridge and achieve ZVS with low turn-off current over a wide range of coupling coefficient.

The design process and control strategy of the entire system are shown in Fig. 1. First, the appropriate $x_u$ and $x_c$ are given to determine the input voltage and capacitance to complete the system hardware design. In this case, sub-resonant frequency control can be implemented by using a PI controller to regulate the output power. The difference between PI output and resonant frequency of pickup side is used as the operating freqeuncy to directly generate the corresponding pulse to control the H-bridge converter. This indicates that the sub-resonant frequency control is a very easy to implement but effective method, which is considered particularly suited for high-power battery charging applications during large variations in coupling conditions.

While the design method and operating strategy leading to the characteristics shown in Fig. 3 were introduced in [8]-[11], the efficiency characteristics were not explicitly or quantitatively evaluated. Indeed, it is important to ensure high efficiency for high power IPT systems independently of the operating conditions, since the losses directly impact the reliability and cooling requirements, and thereby also the achievable power density. These factors contribute to the total system cost and practical applicability. Thus, efficiency should be accurately evaluated over the entire intended operating range.

## III. EFFICIENCY ANALYSIS OF SS COMPENSATED IPT SYSTEM FOR SUB-RESONANT OPERATION

The efficiency of IPT system with sub-resonant frequency control is analyzed in this section, while the system is regulated at the rated power. To analyze the losses in the IPT system clearly and in detail, they are divided in two parts: losses in resonant network and converters (include H-bridge and diode rectifier). Moreover, the efficiency of IPT systems with the sub-resonant frequency control method and the losses with phase

TABLE I
PARAMETERS OF SIMULATED IPT-SYSTEM

| General parameters | Values |
| --- | --- |
| Nominal power, $P_0$ | 240 W |
| Nominal receiving voltage, $V_2$ | 40 V |
| Nominal Coupling factor, $k_{nom}$ | 0.2 |
| pickup coil resonant frequency, $f_r$ | 140.0 kHz |
| Self-inductance, $L_1, L_2$ | 30.63, 30.48 $\mu H$ |
| Quality factor, $Q_1, Q_2$ | 510, 490 |
| Unbalanced factor, $xu$ | 0.98 |
| Detuning factor, $xc$ | 1.03 |
| Semiconductor devices (H-bridge and rectifier) | IRFS4010 |

shift modulation for conventional voltage control at the resonance frequency are compared in this section.

### A. Efficiency Analysis of the Resonant Network

The maximum achievable power transfer efficiency of the IPT system shown in Fig. 2 can be expressed as [12]:

$$\eta_{max} = \frac{k^2 Q^2}{(1+\sqrt{1+k^2Q^2})^2} \tag{3}$$

where $Q = \sqrt{Q_1 \cdot Q_2} = \sqrt{\dfrac{\omega_0 L_1}{R_1} \dfrac{\omega_0 L_2}{R_2}}$

The maximum efficiency of the conventional SS-IPT system is only achieved when the system is operated at resonance and the equivalent load at the pickup is perfectly matched to the reflected impedance given by:

$$R_{eq} = \frac{V_2^2}{P_{out}} = R_2\sqrt{1+k^2Q^2} \tag{4}$$

Although unbalanced factor and detuning factor are introduced in sub-resonant frequency control, they are very close to 1 and will not significantly influence the maximum achievable efficiency. Therefore, the rated output power $P_{out}$, constant pickup voltage $V_2$ and nominal coupling coefficient $k_{nom}$ of the IPT system can be designed according to equation (4). Then the coil efficiency can be expressed as:

$$\eta_{TE} = \frac{V_2 I_2}{V_2 I_2 + I_1^2 R_1 + I_2^2 R_2} \tag{5}$$

In this case, the transfer efficiency of resonant network with sub-resonant operation are shown in Fig. 4 by using equations (1), (4) and (5). It is easy to find that the efficiency of the operating points ($P_1$, $P_2$ and $P_3$) with rated power maintains constant, which is equal to the maximum efficiency as designed at $k_{nom}$. Moreover, when the efficiency of IPT system operating at high $k$ is higher than the maximum efficiency value at $k_{nom}$, the corresponding operating power of the system is lower than the rated power as shown in Fig. 3.

As mentioned above, the system can regulate the rated power flow with sub-resonant frequency control when $k$ varies widely. In order to better show the system efficiency with changing $k$ values, Fig. 5 can be obtained by using parameters in Table I and substituting $P_{out}$=$P_{rated}$ into (1) and (5). It can be seen from
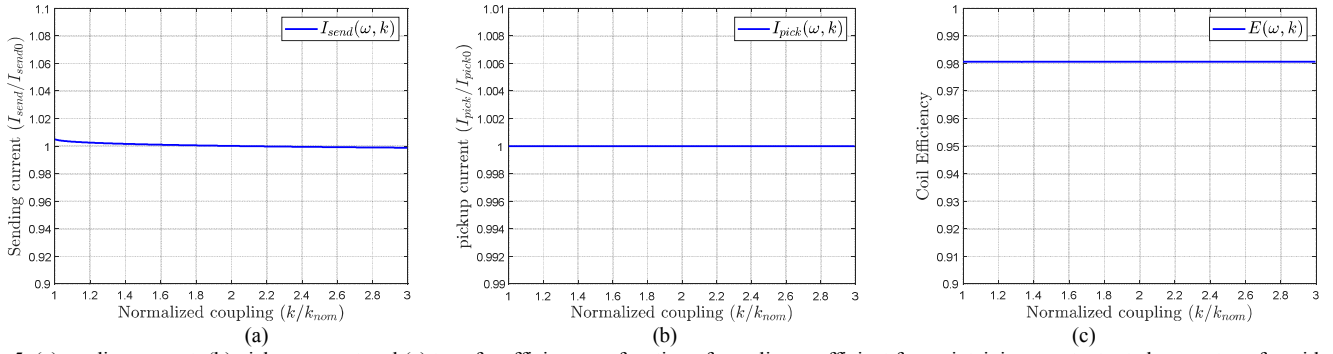
Fig. 5. (a) sending current, (b) pickup current and (c) transfer efficiency as function of coupling coefficient for maintaining constant rated power transfer with sub-resonant frequency control.
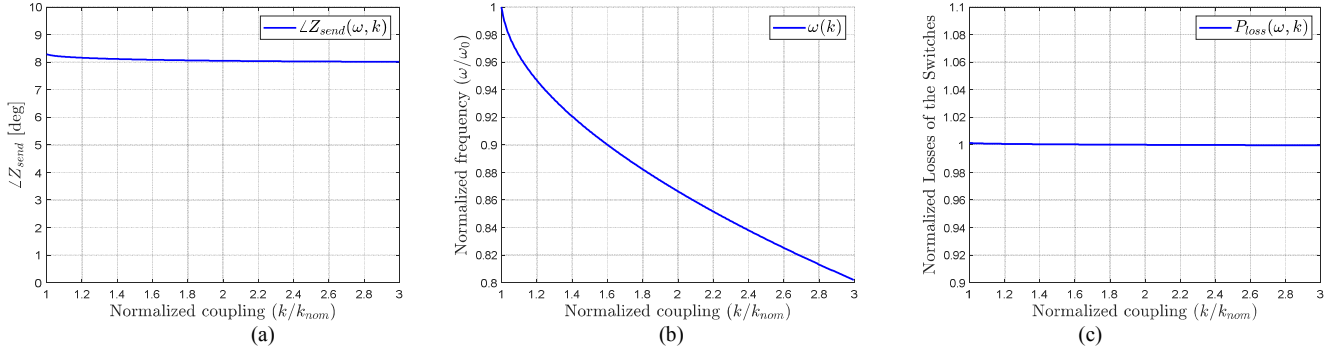


Fig. 6. (a) angle of the input impedance, (b) oprating frequency and (c) total losses of the switches as function of coupling coefficient for maintaining constant rated power transfer with sub-resonant frequency control.

Fig. 5(a) and Fig. 5(b) that the magnitude of the sending current and pickup current remains almost constant, resulting in constant coil transfer efficiency of the IPT system over a wide range of coupling coefficients. The coil efficiency of the IPT system with sub-resonant frequency control method is almost the highest under the conditions of constant rated power and I/O voltages, because of maintaining an almost constant input impedance angle. Moreover, the I/O currents of the IPT system are always the same as for the maximum system efficiency achieved at $k_{nom}$.

### B. Analysis of the Losses in the Inverter and Rectifier

The losses of the switches in the H-bridge and rectifier contain two parts: the conduction losses and switching losses. To analyze the switching losses clearly, the angle of the input impedance $\varphi_1$ and operating frequency required for maintaining constant power transfer with sub-resonant frequency control are shown as function of the coupling coefficient in Fig. 6(a) and 6(b), respectively. By applying these curves, the total losses in the H-bridge and diode rectifier can be calculated. For sub-resonant frequency control, the body diodes of the H-bridge will only conduct during the dead time, so conduction losses of the H-bridge is mainly caused by the MOSFETs and can be obtained by:

$$P_{con\_H} = 2I_1^2 R_{Mos\text{-}on} \qquad (6)$$

where $R_{Mos\text{-}on}$ is the equivalent on-state resistance of MOSFETs.

Regarding the switching losses of the H-bridge, it can be

seen from Fig. 6(a) that the slightly inductive operation of the H-bridge is achieved, resulting in ZVS with low turn-off current of all H-bridge switches. In this case, turn-on losses can be avoided completely. Moreover, the gate drive circuitry can generally turn-off the semiconductor before the drain-source voltage rises due to the low turn-off input currents, which leads to the negligible turn-off losses ($e_{SW\text{-}OFF}$) compared to the conduction losses of the IPT system [13].

For the diode rectifier, the total losses mainly consist of the diode conduction losses which are shown as:

$$P_{Con\_D} = 2I_2^2 R_{diod\text{-}on} + \frac{4\sqrt{2}}{\pi} V_T I_2 \qquad (7)$$

where $V_T$ and $R_{diod\text{-}on}$ are the threshold voltage and the equivalent on-state resistance of the rectifier diode, respectively.

Finally, the total power losses of the H-bridge and rectifier for the sub-resonant frequency control can be calculated as:

$$P_{FC\_loss} = 2I_1^2 R_{Mos\text{-}on} + e_{SW\_OFF} + 2I_2^2 R_{diod\text{-}on} + \frac{4\sqrt{2}}{\pi} V_T I_2 \qquad (8)$$

The corresponding result is plotted in Fig. 6(c) by using datasheet parameters of the devices specified in Table I. Because the sine of the input impedance angle is always close to 0 and the sending and pickup currents remain constant, the total losses of switches are almost unchanged as shown in Fig. 6(c).
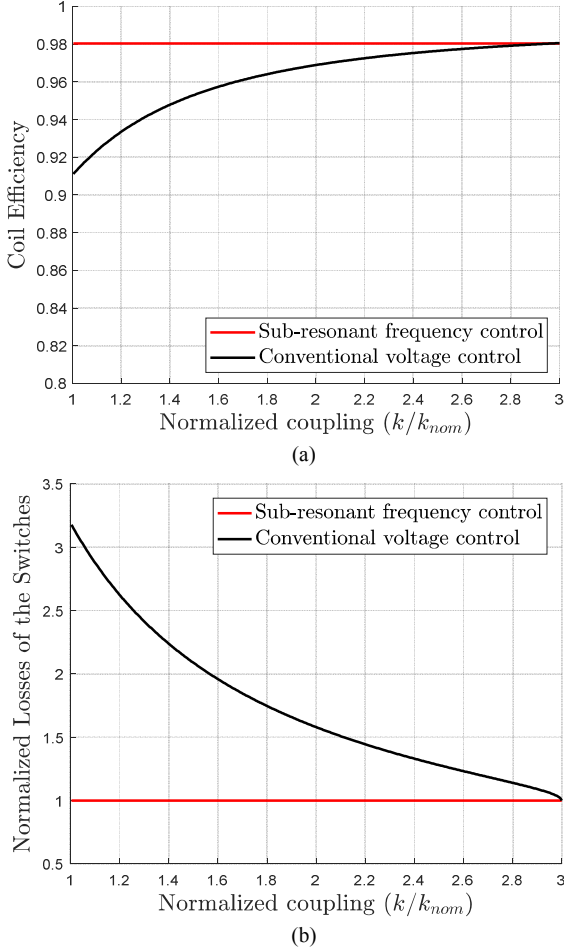
(a)



(b)

Fig. 7. The efficiency comparison of the IPT system with constant output power and voltage load. (a) Coil efficiency (b) total losses of the switches

## C. Comparative Analysis with the IPT System Designed for Voltage Control

The phase shift modulation method, as a well-known voltage control at the resonance frequency, is a more common method to regulate the rated power of the IPT system by controlling sending voltage [14], [15]. To better evaluate the method for sub-resonant frequency control, the efficiency of the above two methods will be compared in this part. In the IPT system designed for the conventional voltage control, the system operated at fixed frequency is designed with ideal balance and is perfectly tuned: $x_u=x_c= 1.0$. Besides, it is assumed that the same coil design and maximum I/O dc voltages are used for both systems. When considering that the variation range of the coupling coefficient is from 0.2 to 0.6, the resonant frequency of the voltage control should be designed as equation (9) to keep the same rated power and maximum I/O dc voltage as that of sub-resonant frequency control.

$$f_r' = \frac{k_{nom}}{k_{max}} \cdot f_r = \frac{f_r}{3} \qquad (9)$$

Moreover, in order to maintain the rated power of the IPT system with different coupling conditions, the sending voltage should be controlled as:
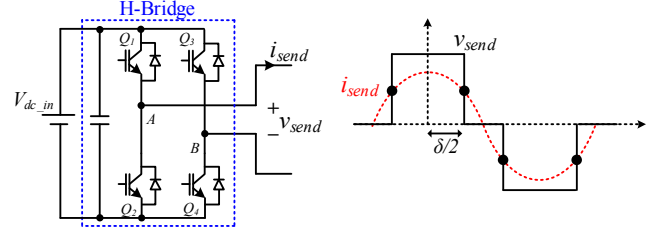


Fig. 8. H-Bridge converter and output waveforms under phase shift modulation.

$$v_1 = \sqrt{\frac{P_{nom} \cdot (R_1 \cdot (R_2 + R_{eq}) + \omega_0^2 M^2)^2}{\omega_0^2 M^2 R_{eq}}} \qquad (10)$$

Then the sending coil current and the pickup coil current of the IPT system with voltage control can be easily calculated. Based on equation (5), the transfer efficiency of the resonant network of both the systems are shown in Fig. 7(a). Compared with the constant efficiency obtained with sub-resonant frequency control, the efficiency of voltage control is lower over a wide range of coupling and will decrease as $k$ decreases.

The losses of the switches of both systems are also completely different. The conventional voltage control has a phase shift angle $\delta$ shown as Fig. 8, which will affect the conduction losses and switching losses of the MOSFETs and body diodes of the H-bridge. The total losses of the switches have been calculated in reference [16] and shown as:

$$P_{VC\_loss} = \frac{1}{\pi} I_1^2 R_{H-diod-on} (\pi - \delta - \sin\delta) + \frac{2\sqrt{2}}{\pi} V_{H-T} I_1 (1 - \sin\frac{\delta}{2})$$

$$+ \frac{1}{\pi} I_1^2 R_{Mos-on} (\pi + \delta + \sin\delta) + 2 I_2^2 R_{diod-on} + \frac{4\sqrt{2}}{\pi} V_T I_2 \qquad (11)$$

$$+ 2\sqrt{2} V_{ds} I_1 \cos(\frac{\delta}{2}) \times (\frac{e_{SW\_ON} + e_{SW\_OFF}}{V_R I_R} + \frac{Q_{RR}}{I_{R\_D}}) \times f_r'$$

where $V_R$ and $I_R$ are the rated drain-source voltage and source current of MOSFET; $e_{SW\_ON}$ and $e_{SW\_OFF}$ are the rated turn-on and turn-off energy losses of MOSFET; $f_0$ is the operating frequency; $V_{H-T}$ and $R_{H-diod-on}$ are the threshold voltage and the equivalent on-state resistance of the body diode of MOSFETs of the H-bridge, respectively; $Q_{RR}$ and $I_{R\_D}$ are the reverse recovery charge and the rated current of the body diode of the H-bridge. During the non-phase shift angle period of voltage control, the body diodes of the H-bridge will conduct, causing its conduction losses to be different from that of sub-resonant frequency control. According to equation (8) and (11), the total losses of the switches of both systems are shown in Fig. 7(b). Compared with sub-resonant frequency control, the total losses of switches of voltage control are higher over a wide range of coupling and will increase as $k$ decreases. Only when the IPT system is working around the highest coupling $k_{max}$, will the coil losses and converter losses of the voltage-controlled IPT system be close to what is achieved with the sub-resonant frequency-controlled IPT system. However, it is worth noting that the losses of the parasitic output capacitance ($C_{oss} \cdot V_{dc}^2$) is not considered in equation (11) when the phase shift angle is π,
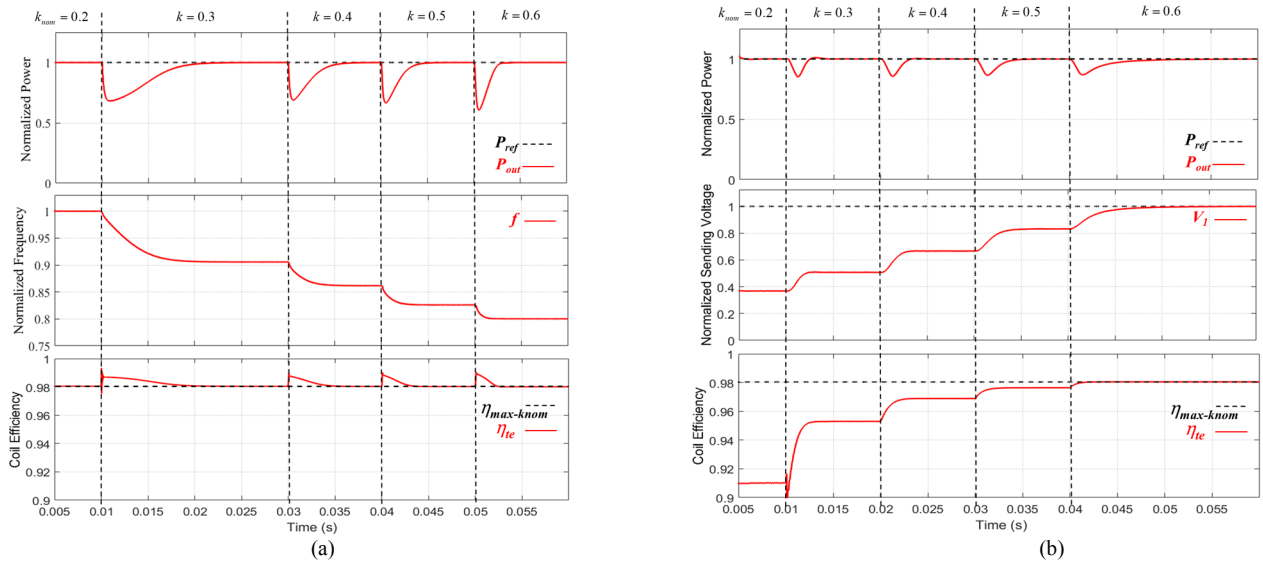
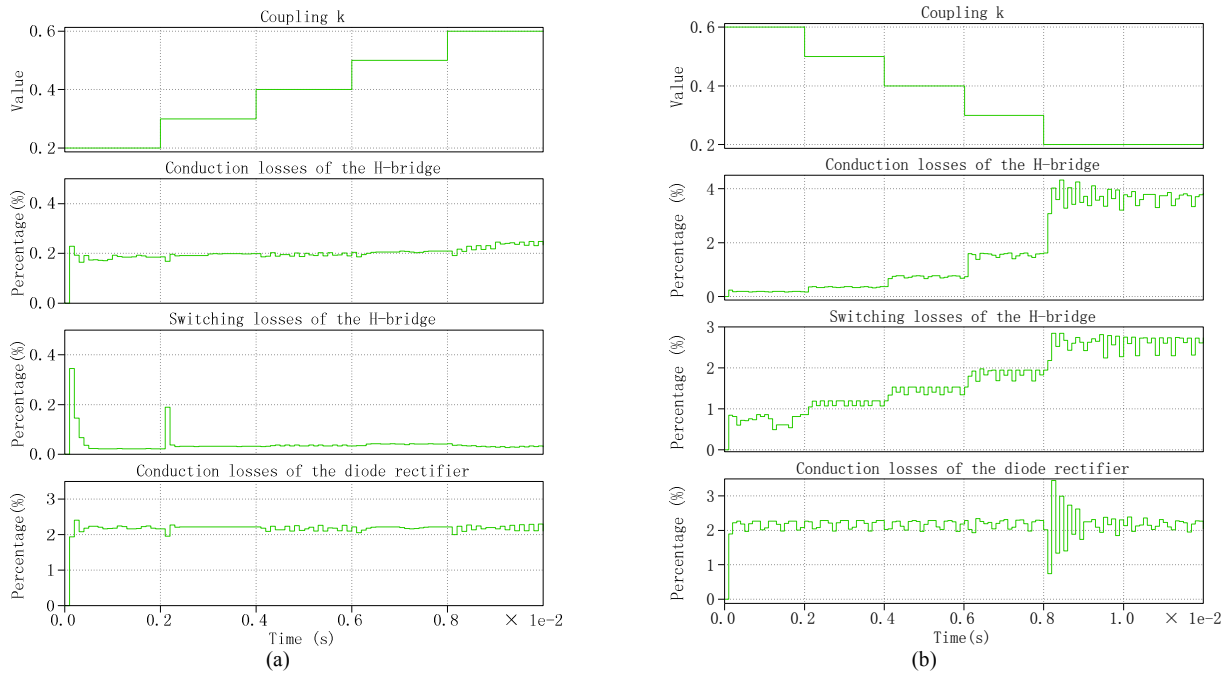Fig. 9. The coil efficiency of the IPT system for the sub-resonant frequency control and the voltage control.



Fig. 10. The percentage of the losses of the convreters to the total power of the IPT system for the sub-resonant frequency control and the voltage control.
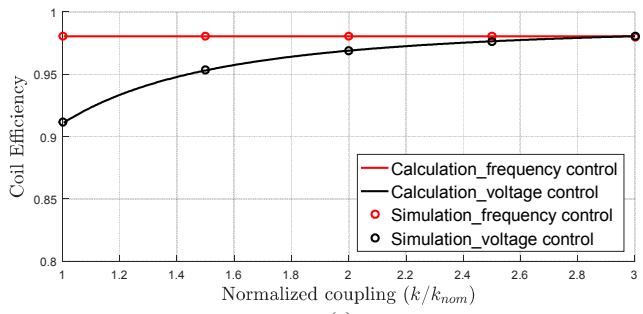
so the efficiency of both methods is the same at the $k_{max}$ point. If the voltage-controlled IPT system does not perform additional measures to achieve soft switching, its switching losses at the $k_{max}$ point will still be slightly larger than that under sub-resonant frequency control.
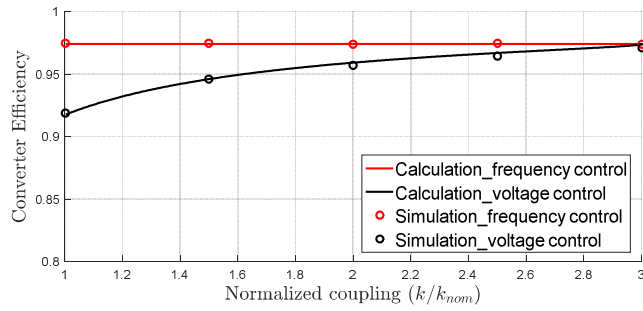
## IV. SIMULATION AND EXPERIMENTAL RESULTS

To verify the effectiveness of the presented efficiency analysis for the IPT system with sub-resonant frequency control, a Simulink/PLECS model is implemented, and a low-power laboratory prototype is also built. The system specifications are listed in Table I.
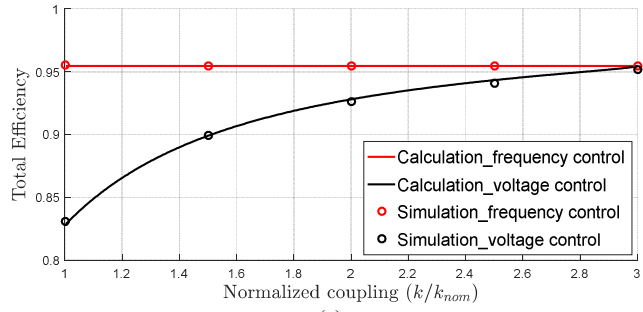
### A. Simulation Results

In the simulations, the main circuit is completed .in PLECS, and its thermal modeling is built according to the datasheet of the MOSFET shown in Table I to calculate the device losses [17]. The control model of the IPT system is implemented in Simulink. Fig. 9 shows the coil efficiency of the IPT system at different $k$ under sub-resonant frequency control and voltage control. As expected, when the IPT system with sub-resonant frequency control is operating at the rated power, the coil efficiency in steady-state conditions remains constant even with large variations in coupling conditions. However, the coil efficiency of the IPT system with voltage control decreases for low values of $k$. Moreover, the efficiency of the IPT system with voltage control at the $k_{max}$ point is the same as that of the sub-

Fig. 11. The efficiency comparison of the IPT system with the sub-resonant freuqency control and the voltage control: (a) coil efficiency, (b) converter efficiency and (c) total efficiency.
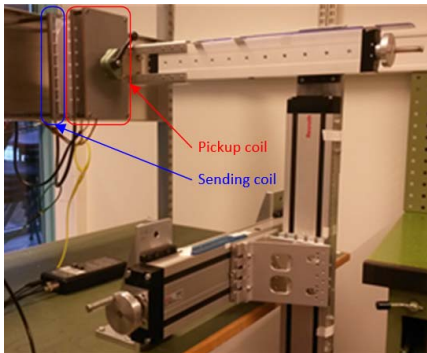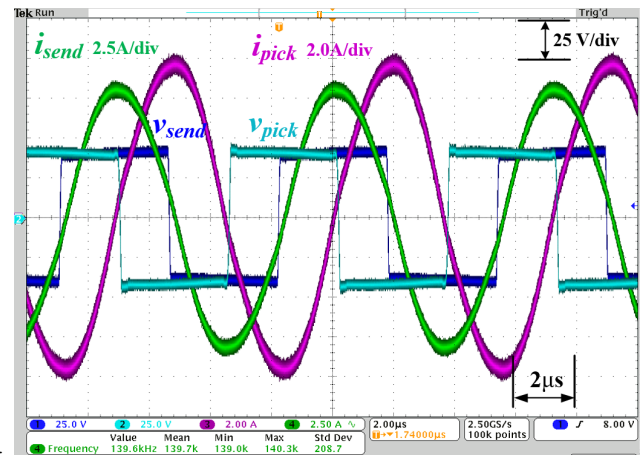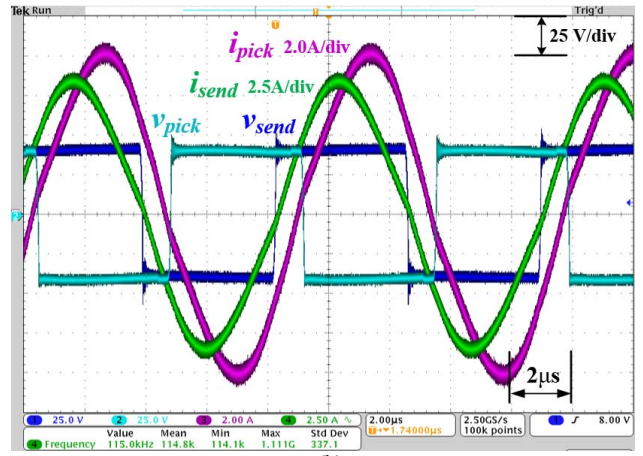


Fig. 12. Experimental setup of the IPT system

Fig. 13. IPT system operated at rated I/O voltage and output power. (a) $k = k_{nom} = 0.23, f = f_0 = 140\text{kHz}$ ; (b) $k = 2 \cdot k_{nom} = 0.46, f = 115\text{kHz}$ ;
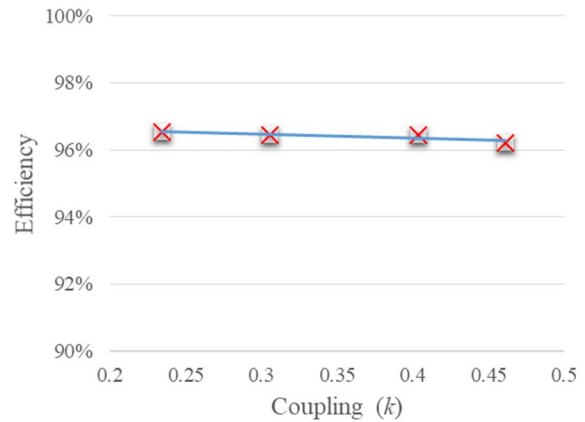


Fig. 14. The efficiency of the IPT system operated at rated output power with different coupling $k$.

resonant frequency controlled IPT system, but it is significantly reduced at the $k_{min}$ point. To demonstrate the efficiency of the converters, the conduction losses and switching losses are shown in detail in Fig. 10. The losses of the switches under sub-resonant frequency control remains almost unchanged, while the losses of the H-bridge under voltage control increase sharply with the decrease of coupling $k$. In order to compare the system

efficiency of both methods clearly, Fig. 11 shows the calculated results and simulation results of the coil efficiency, the converter efficiency (include H-bridge and rectifier), and the total efficiency of the IPT system. It can be seen from Fig. 11(a) that the calculated results of the coil efficiency are completely consistent with the simulation results, while the calculated results of the converter efficiency shown in Fig. 11(b) are

relatively close to the simulation results, with an error of less than 0.3% at the high $k$. This is because some factors such as temperature and parasitic output capacitance losses are not considered in the calculation, and the conduction and switching losses of the converter with different input currents are estimated. In general, the calculated results and the simulation results match very well in a large range. At $k_{max}$, the total efficiency of the voltage-controlled IPT system is almost the same as that of the frequency-controlled IPT system, whose maximum efficiency is 95.45%. With the decrease of $k$, the total efficiency of the voltage-controlled IPT system is greatly reduced, which is 12% lower than the efficiency of the frequency-controlled IPT system at $k_{min}$.

## B. Experimental Results

In order to further prove the results from the analysis and simulations, the efficiency of a laboratory prototype as shown in Fig. 12 designed for off-resonant frequency control has been evaluated. The dc side of the prototype was a DC power supply, and the battery charging system was emulated by an electronic constant voltage load. Because the conduction losses of the diode is much higher than the losses of the MOSFET, the diode rectifier was replaced by a MOSFET synchronous rectifier in the experiments. In this case, the constant pickup voltage/current has not been changed compared with the operation condition of using a diode rectifier. Other parts such as control and design remain unchanged. The synchronous rectifier just reduces the constant conduction losses of diodes. Therefore, the efficiency of the experimental prototype under different $k$ values can also be used to verify the effectiveness of the above theoretical analysis. Fig. 13 shows the sending/pickup voltages/currents waveforms of the IPT system working at $k_{nom}$ and $k_{max}$. It can be seen that the sending side and pickup side of the above two cases are slightly inductive to achieve ZVS with low turn-off current. Moreover, Fig. 14 shows the efficiencies of the IPT system with sub-resonant frequency control at different $k$, which are almost constant and equal to the maximum efficiency value (96.45%) at $k_{nom}$. The experimental efficiency is slightly higher than the simulation results because the conduction losses of diodes are greatly reduced as described above. These simulation and experimental results confirm the conclusions drawn in the previous section.

## V. Conclusion

The detailed efficiency analysis of an IPT system designed for sub-resonant frequency control during large variations in coupling conditions is presented in this paper. The transfer efficiency of the resonant network of the IPT system at rated power maintains constant independently of the coupling. Moreover, the angle of input impedance under the sub-resonant frequency control is slightly inductive over a wide range of coupling coefficient, leading to ZVS. Thus the losses of the switches are minimum, and remain almost unchanged. Compared with the losses of the IPT system with the conventional voltage control at the resonant frequency, the losses of the resonant network and converters by sub-resonant

frequency control are much lower, especially in the case of low $k$. Simulink/PLECS-based simulations and experiments on a small-scale prototype demonstrate the validity of the theoretical analysis and obtained conclusions.

## References

[1] G. A. Covic and J. T. Boys, "Modern trends in inductive power transfer for transport applications," *IEEE J. Emerg. Sel.Topics Power Electron.*,vol. 1, no. 1, pp. 28–41, Mar. 2013.

[2] C. T. Rim and C. Mi, Wireless power transfer for electric vehicles and mobile devices. John Wiley & Sons, 2017.

[3] G. Guidi, J. A. Suul, F. Jenset, and I. Sorfonn, "Wireless charging for ships: high-power inductive charging for battery electric and plug-in hybrid vessels," *IEEE Electr. Mag.*, vol. 5, no. 3, pp. 22–32, 2017.

[4] J. H. Kim *et al.* "Development of 1-MW inductive power transfer system for a high-speed train," *IEEE Trans. Ind. Electron.*, vol. 62, no. 10, pp. 6242–6250, Oct. 2015.

[5] S. Y. Choi, B. W. Gu, S. Y. Jeong, and C. T. Rim, "Advances in wireless power transfer systems for roadway-powered electric vehicles," *IEEE J. Emerg. Sel. Topics Power Electron.*, vol. 3, no. 1, pp. 18–36, Mar. 2015.

[6] X. Zhang et al., "A Control Strategy for Efficiency Optimization and Wide ZVS Operation Range in Bidirectional Inductive Power Transfer System," *IEEE Trans. Ind. Electron.*,, vol. 66, no. 8, pp. 5958-5969, Aug. 2019.

[7] H. Li, J. Fang, S. Chen, K. Wang, and Y. Tang, "Pulse density modulation for maximum efficiency point tracking of wireless power transfer systems," *IEEE Trans. Power Electron.*, vol. 33, no. 6, pp. 5492–5501, Jun. 2018.

[8] G. Guidi, J. A. Suul, "Minimization of Converter Ratings for MW-scale Inductive Charger Operated under Widely Variable Coupling Conditions," in *Proceedings of the IEEE PELS Workshop on Emerging Technologies: Wireless Power*, 2015 WoW, Daejeon, Korea, 5-6 June 2015, pp. 1-7.

[9] G. Guidi and J. A. Suul, "Minimizing converter requirements of inductive power transfer systems with constant voltage load and variable coupling conditions," *IEEE Transactions on Industrial Electronics*, vol. 63, no. 11, pp. 6835–6844, Nov 2016.

[10] G. Guidi and J. A. Suul, "Modelling techniques for designing high performance on-road dynamic charging systems for electric vehicles," in *Proc. 31st Int. Electric Vehicle Symposium and Exhibition & Int Electric Vehicle Technology Conf.*, Sep. 2018, pp. 1–7.

[11] E. Torsgård, G. Guidi, J. A. Suul, "Small-Signal State-Space Analysis of Inductive Battery Charging System in Off-Resonant Operation," in *Proceedings of the Twentieth IEEE Workshop on Control and Modelling for Power Electronics, COMPEL 2019*, Toronto, Ontario, Canada, 17-20 June 2019, pp 1-8.

[12] S. Li and C. C. Mi, "Wireless power transfer for electric vehicle applications," *IEEE J. Emerg. Sel. Topics Power Electron.*, vol. 3, no. 1, pp. 4–17, Mar. 2015.

[13] Matthias Kasper, Ralph M. Burkart, Gerald Deboy and Johann W. Kolar, "ZVS of Power MOSFETs Revisited" *IEEE Transactions on Power Electron.*, vol. 31, no. 12, pp. 8063–8067, Dec. 2016.

[14] Kai Song, Zhenjie Li, Jinhai Jiang and Chunbo Zhu , "Constant Current/Voltage Charging Operation for Series–Series and Series–Parallel Compensated Wireless Power Transfer Systems Employing Primary-Side Controller," *IEEE Trans. Power Electron.*, vol. 33, no. 9, pp. 8065–8080, Sep. 2018.

[15] T. Diekhans and R. W. De Doncker, " A dual-side controlled inductive power transfer system optimized for large coupling factor variations and partial load," *IEEE Trans. Power Electron.*, vol. 30, no. 11, pp. 6320–6328, Nov. 2015.

[16] Yong Li, Jiefeng Hu, Feibin Chen, Zilin Li, Zhengyou He, and Ruikun Mai, "Dual-Phase-Shift Control Scheme With Current-Stress and Efficiency Optimization for Wireless Power Transfer Systems," *IEEE Transactions on Circuits and System I: Regular Papers*, vol. 65, no. 9, pp. 3110-3121, Sep. 2018.

[17] The Datasheet of the MOSFET IRFS4010, Available online: https://www.infineon.com/dgdl/irfs4010-7ppbf.pdf?fileId=5546d462533600a401535636c33c2185, Oct. 2008.